

Ultrafast Lateral Photo-Dember Effect in Graphene Induced by Nonequilibrium Hot Carrier Dynamics

Chang-Hua Liu,^{†,⊥} You-Chia Chang,^{‡,§} Seunghyun Lee,^{†,||} Yaozhong Zhang,^{||} Yafei Zhang,^{||} Theodore B. Norris,^{*,†,‡} and Zhaohui Zhong^{*,†,‡}

[†]Department of Electrical Engineering and Computer Science, University of Michigan, Ann Arbor, Michigan 48109, United States

[‡]Center for Photonics and Multiscale Nanomaterials, University of Michigan, Ann Arbor, Michigan 48109, United States

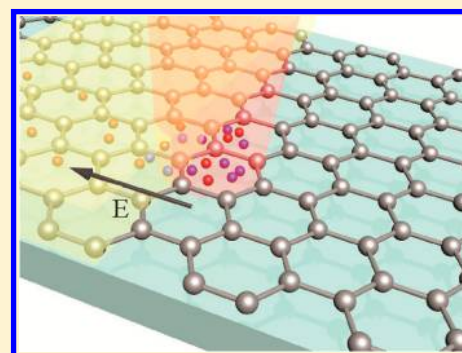
[§]Department of Physics, University of Michigan, Ann Arbor, Michigan 48109, United States

^{||}Key Laboratory for Thin Film and Microfabrication of the Ministry of Education, Research Institute of Micro/Nano Science and Technology, Shanghai Jiao Tong University, 800 Dongchuan Road, Shanghai 200240, China

Supporting Information

ABSTRACT: The photo-Dember effect arises from the asymmetric diffusivity of photoexcited electrons and holes, which creates a transient spatial charge distribution and hence the buildup of a voltage. Conventionally, a strong photo-Dember effect is only observed in semiconductors with a large asymmetry between the electron and hole mobilities, such as in GaAs or InAs, and is considered negligible in graphene due to its electron–hole symmetry. Here, we report the observation of a strong lateral photo-Dember effect induced by nonequilibrium hot carrier dynamics when exciting a graphene–metal interface with a femtosecond laser. Scanning photocurrent measurements reveal the extraction of photoexcited hot carriers is driven by the transient photo-Dember field, and the polarity of the photocurrent is determined by the device’s mobility asymmetry. Furthermore, ultrafast pump–probe measurements indicate the magnitude of photocurrent is related to the hot carrier cooling rate. Our simulations also suggest that the lateral photo-Dember effect originates from graphene’s 2D nature combined with its unique electrical and optical properties. Taken together, these results not only reveal a new ultrafast photocurrent generation mechanism in graphene but also suggest new types of terahertz sources based on 2D nanomaterials.

KEYWORDS: Graphene, photocurrent, hot carriers, photo-Dember effect



The photo-Dember effect is a transient dipole radiation process which can be demonstrated through exciting a freestanding bulk GaAs¹ (electron mobility $\mu_e = 8500 \text{ cm}^2 \text{ V}^{-1} \text{ s}^{-1}$, hole mobility $\mu_h = 400 \text{ cm}^2 \text{ V}^{-1} \text{ s}^{-1}$) or InAs^{2,3} ($\mu_e = 30000 \text{ cm}^2 \text{ V}^{-1} \text{ s}^{-1}$, $\mu_h = 240 \text{ cm}^2 \text{ V}^{-1} \text{ s}^{-1}$) with a femtosecond laser (Figure 1a). Due to an inherent asymmetry in the mobility, excited hot electrons and holes will diffuse from the surface into the bulk with different velocities. The resulting spatial charge separation builds up a transient photo-Dember field, corresponding to a transient dipole perpendicular to the excitation surface, which can radiate into the far field.

With shrinking material dimensions, the ultrafast dynamics of the light–matter interaction can be modified by quantum confinement effects. Graphene, in particular, is a 2-dimensional material with high carrier mobility as well as broadband and strong light coupling.^{4,5} Initial ultrafast studies have not only probed the carrier dynamics of graphene from the femtosecond to picosecond time scales^{6–8} but have also unveiled important hot carrier physics including hot carrier diffusion,⁹ nonlinear photoluminescence,^{10,11} photothermoelectric effects,¹² and hot carrier extraction.¹³ The hot carrier diffusion originated photo-

Dember effect was thought to be trivially absent in graphene,¹⁴ due to strong electron–hole symmetry.^{9,14}

We demonstrate in this Letter that, contrary to the conventional wisdom, a high photocarrier temperature in graphene can compensate for the small electron–hole mobility difference, leading to an intense lateral photo-Dember field. This can be understood via Figure 1b in combination with the following key properties. First, the incident light is partially shadowed by a metal electrode, establishing a strong photocarrier density gradient near the metal/graphene edge. This sharp gradient, together with 2D spatial confinement, causes efficient lateral diffusion of hot carriers into the metal-covered area.^{15,16} Second, the low electronic specific heat capacity in graphene favors a high carrier temperature following excitation.¹⁰ This, combined with high carrier mobility, will enhance the diffusion speed of hot carriers, as given by the Einstein relation⁹

Received: May 15, 2015

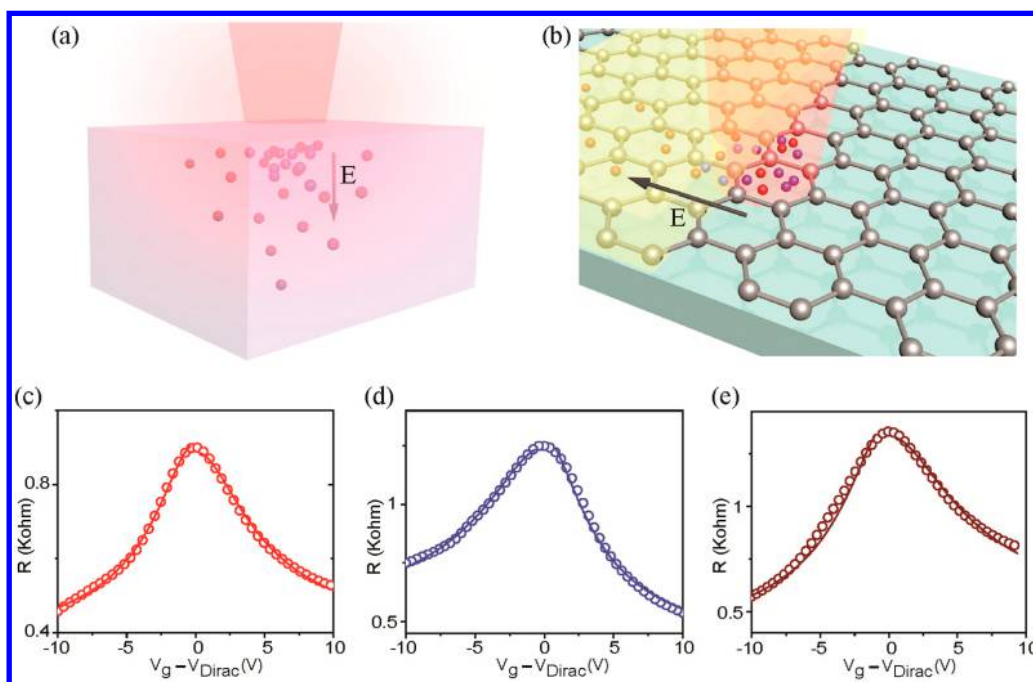


Figure 1. Lateral photo-Dember effect in graphene induced by nonequilibrium hot carrier dynamics. (a) Schematic of the formation of conventional photo-Dember field in bulk semiconductors. Electrons and holes are represented by red and blue spheres, respectively. (b) Schematic of the formation of lateral photo-Dember field at the metal/graphene interface. A sharp carrier density gradient at the contact edge and 2D nature of graphene induce hot carrier diffusion parallel to the excited plane. (c)–(e) Resistance as a function of gate voltage (round symbols) and its fitting (solid line) of (c) device A (red), (d) device B (blue), and (e) device C (brown).

Table 1. Electrical Properties of the Graphene Transistors^a

	mobility ($\text{cm}^2 \text{V}^{-1} \text{s}^{-1}$)			contact metal
	μ_e	μ_h	E_f^0 (eV)	
device A	1095	1289	4.72	titanium
device B	820	611	4.28	titanium
device C	751	925	4.75	palladium

^a μ_e , electron mobility; μ_h , hole mobility; E_f^0 , intrinsic Fermi level of graphene.

$$D = \frac{\mu k_B T}{2q} \quad (1)$$

where D is the diffusion coefficient, μ the excited charge mobility, T the temperature, and k_B the Boltzmann constant. A high carrier temperature is key to magnifying the difference between electron and hole diffusion. Third, strong light coupling within the single atomic layer⁵ results in ultrahigh photocarrier density in graphene, which can be 1–3 orders higher than other low band gap materials.¹⁷ Taken together, the dynamics of nonequilibrium hot carriers in graphene can lead to a strong lateral photo-Dember field. The lateral photo-Dember effect also accounts for an important new mechanism for photocurrent generation in graphene.

To confirm the formation of a photo-Dember field, we employ a scanning photocurrent spectroscopy technique^{13,18,19} to spatially probe the photocurrent generation from graphene transistors (Supporting Information Figure S1). In particular, we fabricated 15 devices having different electron and hole mobilities and compared their photocurrent responses under femtosecond pulse laser excitation ($\lambda = 800$ nm, 150 fs pulse width, and 76 MHz repetition rate). Three representative graphene devices (A–C) are demonstrated here with the electrical gate response of each device shown in Figure 1c–e,

respectively. For comparison, we extract the electron–hole mobility and intrinsic doping level for all three devices.^{20,21} As shown in Table 1, devices A and C show slightly higher hole mobility than electron mobility, whereas device B shows the opposite. This small asymmetry of electron/hole mobility results from unequal impurity scattering between electrons and holes.^{21–23} Also, both device A and device B are contacted with titanium, and device C is contacted with palladium.

We then explored the photoresponse of these three devices under femtosecond laser excitation under the short-circuit condition ($V_{sd} = 0$ V) and Figure 2a shows the schematic of measurement setup. Figure 2b–d are gate-dependent photocurrent maps measured from devices A, B, and C respectively. By comparing these maps, we not only observe photocurrent generation near the contact edges¹³ (position = 0 and 5 μm) but also observe three major features. First of all, the gate-dependent photocurrent does not show a polarity reversal in all three devices. Second, the polarity of the photocurrent from device B is completely opposite to that of devices A and C. Third, regardless of the photocurrent polarity, the magnitude of the photocurrent peaks near the graphene Dirac point gate voltage and decreases by increasing the doping concentration. These features can also be clearly seen from extracting the gate-dependent photoresponse at the left metal/graphene contact edge (position = 0 μm) from three photocurrent maps (Figure 2e–g). We also emphasize that, all 15 devices we fabricated show the same photocurrent map features as the three representative devices (Supporting Information).

The unusual photoresponse described above provides evidence of a lateral photo-Dember effect. For devices A and C, photoexcited hot holes diffuse faster than hot electrons into the metal-covered area due to the slightly higher hole mobility, building up a transient photo-Dember field. This transient field drives electron carriers to the left contact, resulting in a positive

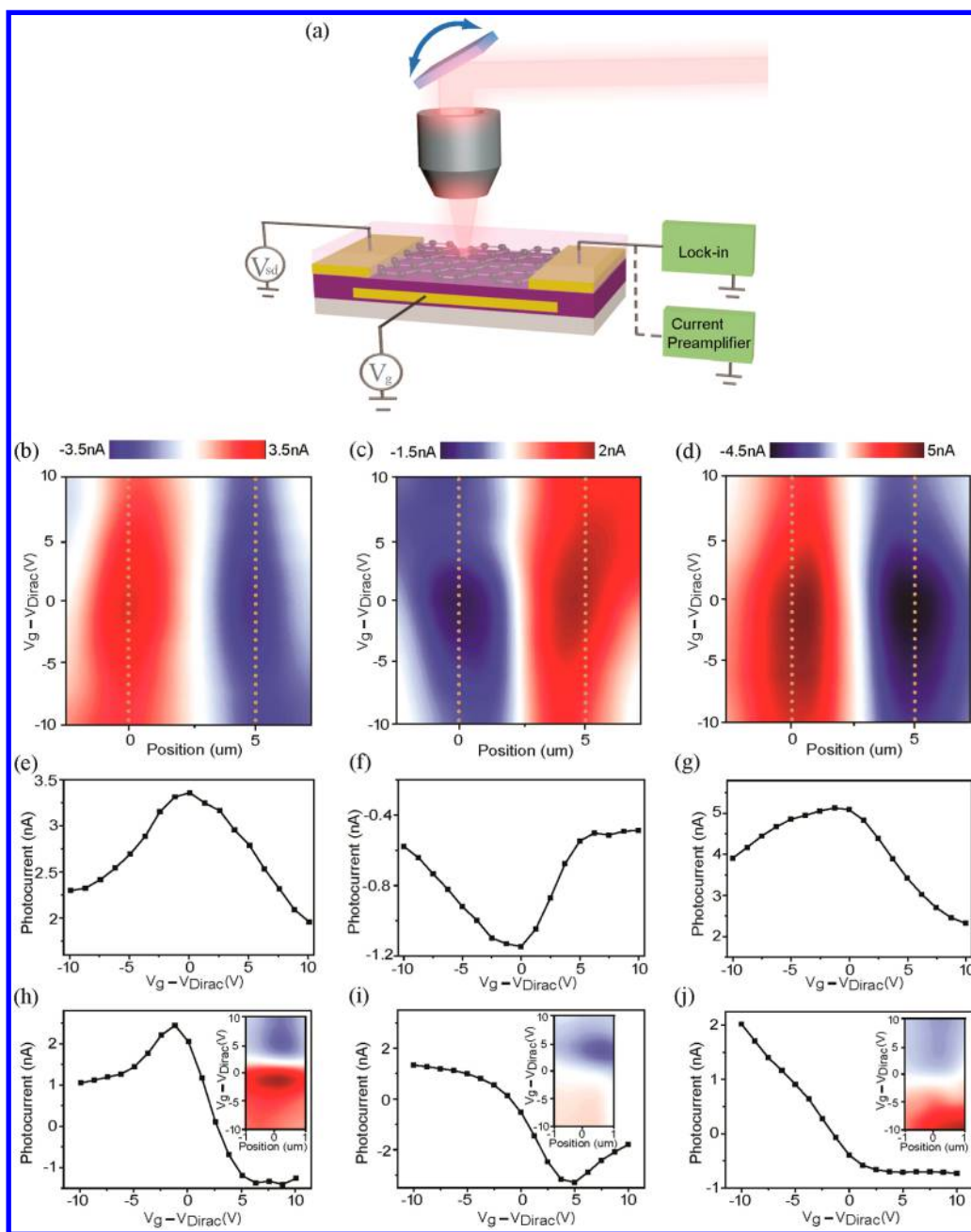


Figure 2. Lateral photo-Dember field drives the extraction of nonequilibrium hot carriers in graphene. (a) Schematic of the scanning photocurrent measurement on a graphene device. The polarity of photocurrent was determined by using a DC current preamplifier, whereas the magnitude of photocurrent was measured by using a lock-in amplifier. (b)–(d) Gate-dependent photocurrent maps under pulse laser excitation measured from (b) device A, (c) device B, and (d) device C, respectively. The excitation pulse energy is ~ 19.7 pJ. The dotted lines at position = 0 and $5 \mu\text{m}$ represent the left and right metal/graphene contact edges. (e)–(g) Extracted gate-dependent photocurrent at the left metal/graphene interface (position = $0 \mu\text{m}$) from (b)–(d), respectively. (h)–(j) Photoresponse of metal/graphene interface under 1.2 mW CW laser excitation. The gate-dependent photocurrent maps (insets) near the left metal/graphene contact and the extracted gate-dependent photocurrent are measured from (h) device A, (i) device B, and (j) device C, respectively. All the scanning photocurrent measurements are conducted at ambient conditions and graphene films are grown by chemical vapor deposition method (ref 38).

photocurrent with the right metal contact grounded. In contrast, device B has a higher electron mobility; hence, the faster electron diffusion leads to a photo-Dember field favoring extraction of hole carriers and a negative photocurrent at the left metal/graphene contact. Regardless of the contact metal and doping concentration of graphene, the polarity of the photocurrent is determined entirely by the electron–hole mobility difference, providing clear evidence for the formation of a lateral photo-Dember field. Moreover, when the photo-

Dember effect dominates the photocurrent generation mechanism, the magnitude of the photocurrent should increase with a longer hot carrier lifetime. This is not only because the duration of the transient field increases with the lifetime but also because maintaining excited carriers at an elevated temperature is central to creating a spatial charge distribution, giving rise to a strong transient field. In fact, a number of theoretical works predict that hot carrier energy relaxation through electron–electron and electron–phonon coupling will

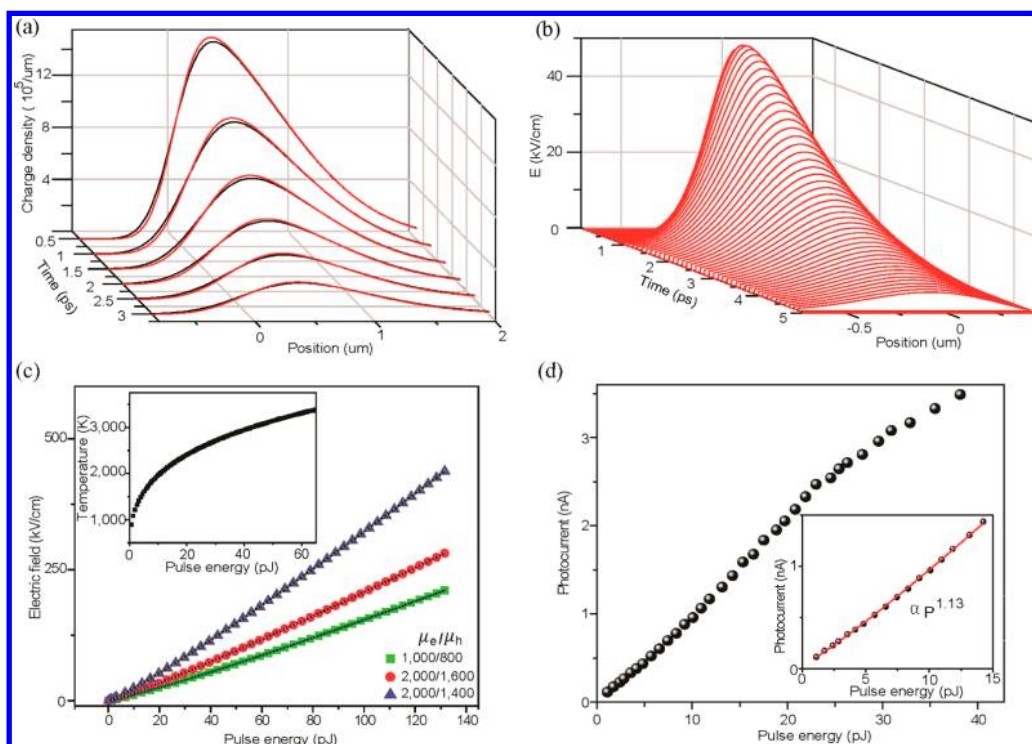


Figure 3. Simulation of lateral photo-Dember field in graphene. (a) Simulation of spatial and temporal evolution of hot electrons (black lines) and holes (red lines) after the pulse laser excitation (26 pJ). Position $< 0 \mu\text{m}$ represents the metal-covered area. (b) Simulation of spatial and temporal evolution of the lateral photo-Dember electric field after the pulse laser excitation (26 pJ). (c) Simulation of power-dependent lateral photo-Dember electric field under different electron–hole mobility (μ_e/μ_h). The unit for mobility is $\text{cm}^2 \text{V}^{-1} \text{s}^{-1}$. Each simulated power-dependent electric field can be fitted by the power law: $E \propto P^{1.13}$ (black lines). The simulated electric field here is at the metal/graphene interface and 1 ps after the pulse excitation. The inset shows the simulated power-dependent hot carrier temperature. (d) Experimental measurement of power-dependent photocurrent from the metal/graphene interface under pulse excitation. The inset shows a zoomed-in view in the low power region.

be faster by increasing the doping concentration in graphene.^{24–27} Our observation of maximum hot carrier photocurrent at the Dirac point agrees with this theoretical prediction.

To compare the hot carrier photocurrent with the near equilibrium carrier photocurrent, we conducted control experiments by measuring the photocurrent at the metal/graphene interface with continuous wave (CW) laser excitation ($\lambda = 900 \text{ nm}$). As shown in Figure 2h–j and the insets, the photoresponse from these three devices consistently exhibits polarity reversal, in agreement with the photovoltaic effect for photocurrent generation at the metal/graphene interface.^{18,19} Importantly, the lack of similar features induced by intense pulse laser indicates steady CW excitation results in low photocarrier temperature and photocarrier density in graphene. Therefore, the photo-Dember field will be insignificant under steady state conditions.

Next, we simulate the hot carrier dynamics and lateral photo-Dember field under pulsed laser excitation by modeling the drift-diffusion equations⁹ (Supporting Information)

$$\frac{\partial n_i}{\partial t} = G \pm \mu_i \frac{\partial(n_i E)}{\partial x} + D_i \frac{\partial^2 n_i}{\partial x^2} - \frac{n_i}{\tau} \quad (2)$$

$$\frac{\partial E}{\partial x} = \frac{q(n_h - n_e)}{\epsilon} \quad (3)$$

where n is the photoexcited carrier density ($i = e, h$ represent electron and hole, respectively), and E is the photo-Dember field. G is the photocarrier generation term. The diffusion

coefficient (D) is related to mobility (μ) via the Einstein relation. Also, we assume hot carrier lifetime $\tau = 1.5 \text{ ps}$,⁷ $\mu_e = 2000 \text{ cm}^2 \text{V}^{-1} \text{s}^{-1}$, and $\mu_h = 1600 \text{ cm}^2 \text{V}^{-1} \text{s}^{-1}$, and for simplicity, we assume hot carriers diffuse in the plane and only in the direction perpendicular to the metal edge due to the sharp carrier gradient. Figure 3a demonstrates the simulated ultrafast diffusion process of hot electrons and holes. Strikingly, the asymmetric carrier distribution near the vicinity of the contact builds up an intense photo-Dember field (Figure 3b). The peak electric field can reach 50 kV cm^{-1} under 26 pJ pulse excitation, exceeding the typical Dember field strength of $< 10 \text{ kV cm}^{-1}$ for bulk semiconductors.^{28,29} Furthermore, our model predicts that increasing the asymmetry of electron–hole mobility as well as device mobility will further enhance the field. We note that the hot carrier mobilities will likely be different than the equilibrium carrier mobilities seen in DC transport measurements, but the asymmetry caused by the scattering responsible for the difference in the low-field mobilities will remain. In addition, the electron–hole symmetry in graphene’s band structure should yield similar hot carrier energy relaxation for electrons and holes. Hence, the difference in DC carrier mobility (and hence diffusion) between electrons and holes will likely remain even at high carrier temperature.

Our simulation also suggests that the field strength increases superlinearly with the pulse energy ($E \propto P^{1.13}$), as shown in Figure 3c. Intuitively, this nonlinear behavior originates from the higher photocarrier density, gradient, and temperature (Figure 3c, inset) together with a higher diffusion coefficient with increasing pulse energy. To experimentally verify the simulation results, we measured the power-dependent photo-

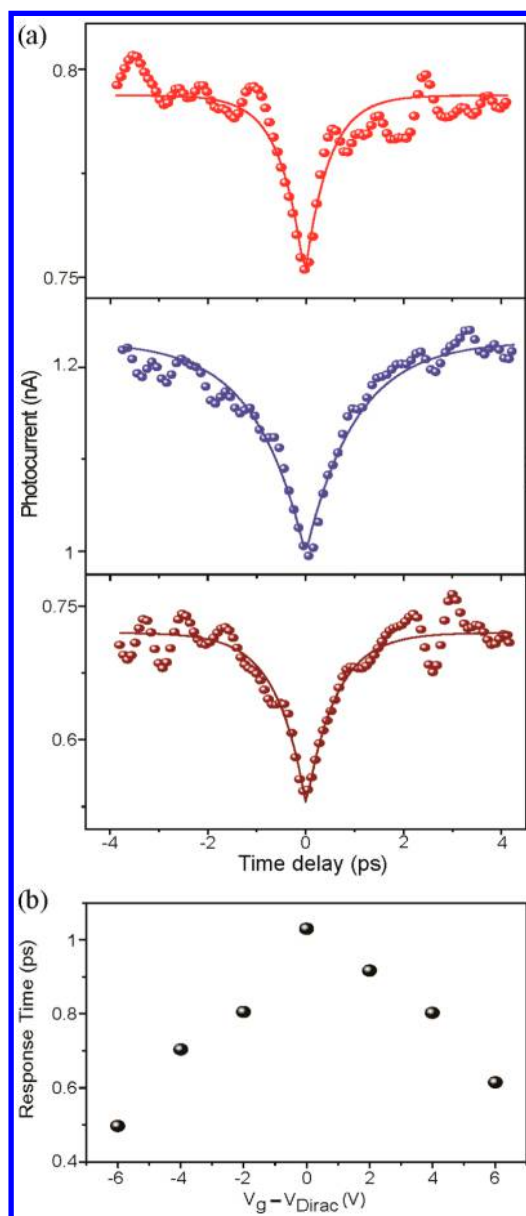


Figure 4. Time resolved ultrafast photoresponse in graphene. (a) Top to bottom: photocurrent versus pump–probe time delay under back gate voltages of $V_g - V_{\text{Dirac}} = -6$ V (red), $V_g - V_{\text{Dirac}} = 0$ V (blue), and $V_g - V_{\text{Dirac}} = 6$ V (brown), respectively. Each measurement is fitted by the single exponential function (solid lines) to extract response time. (b) Response time (τ) as a function of back gate voltage. All the pump–probe measurements are conducted at ambient conditions.

current from the metal/graphene interface. As shown in Figure 3d, the photocurrent grows superlinearly in the low pulse energy region, and then transits to sublinearity under strong excitation due to Pauli blocking.^{30–32} Interestingly, the superlinear region can be fitted well by $I_{\text{pc}} \propto P^{1.13}$ (Figure 3d, inset). Power dependent measurements on two other devices also reveal a similar superlinear trend, with exponents of 1.08 and 1.15, respectively (Supporting Information Figure S4). These results are in excellent agreement with our simulations. We also note that this feature is totally different from power-dependent photocurrent under CW excitation and provides further evidence of the formation of lateral photo-Dember field (Supporting Information Figure S4).

Finally, we employed an ultrafast pump–probe technique¹² to study the effect of doping on hot carrier cooling rate in graphene (Supporting Information Figure S5). On the basis of the drift-diffusion model, the magnitude of photocurrent is closely related to hot carrier concentration via two parameters: diffusion coefficient and hot carrier concentration. Therefore, measuring the photocurrent decay as a function of time delay between two pulses provides a route for probing hot carrier energy relaxation. Figure 4a shows the results of pump–probe measurements under different gate voltages. The presence of a dip at time delay = 0 results from the saturation of the absorption induced by the pump pulse. From each pump–probe result, we extracted the response time and a summary of the gate-dependent response time is shown in Figure 4b (Supporting Information Figure S6). Importantly, the response time reaches a peak value of 1.03 ps at the Dirac point and decreases with increasing electron or hole doping. This result qualitatively agrees with inefficient hot carrier cooling at lower doping concentration^{24,25} and also supports our gate-dependent photoresponse where the photocurrent reaches maximum at the Dirac point.

Our findings reveal an unexpected lateral photo-Dember effect in graphene induced by nonequilibrium hot carriers, providing further insight into the ultrafast photoresponse mechanism in low dimensional materials. The intense lateral transient field could lead to strong out-of-plane terahertz emission, with an inherent advantage over a bulk photo-Dember field where coupling of in-plane terahertz emission is more challenging. Smart engineering of graphene with various substrates to achieve unipolar transport³³ or high carrier mobility,³⁴ coupled with asymmetric electrode design,^{15,16,35} could lead to a new type of graphene based high intensity terahertz source. Furthermore, similar hot carrier dynamics induced lateral photo-Dember effects should exist in other 2D semiconducting nanomaterials, such as monolayer transition metal dichalcogenides^{36,37} (TMDCs). Compared to bulk materials, quantum confinement in 2D nanomaterials may lead to a better alternative for exploiting transient responses for various optical and optoelectronic applications.

■ ASSOCIATED CONTENT

📄 Supporting Information

Detailed device fabrication, scanning photocurrent spectroscopy, gate and power-dependent photocurrents, drift-diffusion simulations, and ultrafast pump–probe spectroscopy. The Supporting Information is available free of charge on the ACS Publications website at DOI: 10.1021/acs.nanolett.5b01912.

■ AUTHOR INFORMATION

Corresponding Authors

*E-mail: tnorris@umich.edu.

*E-mail: zzhong@umich.edu.

Present Addresses

[†]Department of Material Science, Northwestern University, Evanston, Illinois 60208, United States.

[‡]Department of Electrical Engineering, Center for Integrated Systems, Stanford University, Stanford, California 94305, United States.

Author Contributions

C.L. and Z.Z. conceived the experiments. C.L. fabricated the devices; C.L. and Y.C. performed the measurements. All

authors discussed the results; C.L. and Z.Z. cowrote the manuscript and all authors provided comments.

Notes

The authors declare no competing financial interest.

ACKNOWLEDGMENTS

We thank Profs. L. Jay Guo and P. C. Ku for sharing some of their equipment. This work was supported by NSF CAREER Award (ECCS-1254468), the Donors of the American Chemical Society Petroleum Research Fund, NSF Center for Photonic and Multiscale Nanomaterials (DMR-1120923), and the U-M/SJTU Collaborative Research Program in Renewable Energy Science and Technology. Devices were fabricated in the Lurie Nanofabrication Facility at University of Michigan, a member of the National Nanotechnology Infrastructure Network funded by the National Science Foundation.

REFERENCES

- (1) Zhang, X. C.; Xu, J. Z. *Introduction to THz Wave Photonics*; Springer: New York, 2010.
- (2) Gu, P.; Tani, M.; Kono, S.; Sakai, K.; Zhang, X. C. *J. Appl. Phys.* **2002**, *91*, 5533–5537.
- (3) Liu, K.; Xu, J. Z.; Yuan, T.; Zhang, X. C. *Phys. Rev. B* **2006**, *73*, 155330.
- (4) Castro Neto, A. H.; Guinea, F.; Peres, N. M. R.; Novoselov, K. S.; Geim, A. K. *Rev. Mod. Phys.* **2009**, *81*, 109–162.
- (5) Bonaccorso, F.; Sun, Z.; Hasan, T.; Ferrari, A. C. *Nat. Photonics* **2010**, *4*, 611–622.
- (6) Sun, D.; Wu, Z.-K.; Divin, C.; Li, X.; Berger, C.; de Heer, W. A.; First, P. N.; Norris, T. B. *Phys. Rev. Lett.* **2008**, *101*, 157402.
- (7) Dawlaty, J. M.; Shivaraman, S.; Chandrashekhara, M.; Rana, F.; Spencer, M. G. *Appl. Phys. Lett.* **2008**, *92*, 042116.
- (8) Breusing, M.; Ropers, C.; Elsaesser, T. *Phys. Rev. Lett.* **2009**, *102*, 086809.
- (9) Ruzicka, B. A.; Wang, S.; Werake, L. K.; Weintrub, B.; Loh, K. P.; Zhao, H. *Phys. Rev. B* **2010**, *82*, 195414.
- (10) Lui, C. H.; Mak, K. F.; Shan, J.; Heinz, T. F. *Phys. Rev. Lett.* **2010**, *105*, 127404.
- (11) Liu, W.-T.; Wu, S. W.; Schuck, P. J.; Salmeron, M.; Shen, Y. R.; Wang, F. *Phys. Rev. B* **2010**, *82*, 081408.
- (12) Sun, D.; Aivazian, G.; Jones, A. M.; Ross, J. S.; Yao, W.; Cobden, D.; Xu, X. *Nat. Nanotechnol.* **2012**, *7* (2), 114–118.
- (13) Liu, C.-H.; Dissanayake, N. M.; Lee, S.; Lee, K.; Zhong, Z. *ACS Nano* **2012**, *6*, 7172–7176.
- (14) Novoselov, K. S.; Fal'ko, V. I.; Colombo, L.; Gellert, P. R.; Schwab, M. G.; Kim, K. *Nature* **2012**, *490*, 192–200.
- (15) Klatt, G.; Hilser, F.; Qiao, W.; Beck, M.; Gebis, R.; Bartels, A.; Huska, K.; Lemmer, U.; Bastian, G.; Johnston, M. B.; Fischer, M.; Faist, J.; Dekorsy, T. *Opt. Express* **2010**, *18*, 4939–4947.
- (16) Apostolopoulos, V.; Barnes, M. E. *J. Phys. D Appl. Phys.* **2014**, *47*, 374002.
- (17) Palik, E. D. *Handbook of Optical Constants of Solids*; Academic Press: New York, 1985.
- (18) Xia, F.; Mueller, T.; Golizadeh-Mojarad, R.; Freitag, M.; Lin, Y.-M.; Tsang, J.; Perebeinos, V.; Avouris, P. *Nano Lett.* **2009**, *9*, 1039–1044.
- (19) Park, J.; Ahn, Y. H.; Ruiz-Vargas, C. *Nano Lett.* **2009**, *9*, 1742–1746.
- (20) Kim, S.; Nah, J.; Jo, I.; Shahrjerdi, D.; Colombo, L.; Yao, Z.; Tutuc, E.; Banerjee, S. K. *Appl. Phys. Lett.* **2009**, *94*, 062107.
- (21) Chen, J. H.; Jang, C.; Adam, S.; Fuhrer, M. S.; Williams, E. D.; Ishigami, M. *Nat. Phys.* **2008**, *4*, 377–381.
- (22) Hwang, E. H.; Adam, S.; Das Sarma, S. *Phys. Rev. Lett.* **2007**, *98*, 186806.
- (23) Novikov, D. S. *Appl. Phys. Lett.* **2007**, *91*, 102102.
- (24) Tse, W.-K.; Das Sarma, S. *Phys. Rev. Lett.* **2007**, *99*, 236802.
- (25) Song, J. C. W.; Tielrooij, K. J.; Koppens, F. H. L.; Levitov, L. S. *Phys. Rev. B* **2013**, *87*, 155429.
- (26) Bistritzer, R.; MacDonald, A. H. *Phys. Rev. Lett.* **2009**, *102*, 206410.
- (27) Malic, E.; Winzer, T.; Bobkin, E.; Knorr, A. *Phys. Rev. B* **2011**, *84*, 205406.
- (28) Ascazubi, R.; Shneider, C.; Wilke, I.; Pino, R.; Dutta, P. S. *Phys. Rev. B* **2005**, *72*, 045328.
- (29) Nakajima, M.; Hangyo, M.; Ohta, M.; Miyazaki, H. *Phys. Rev. B* **2003**, *67*, 195308.
- (30) Bao, Q.; Zhang, H.; Wang, Y.; Ni, Z.; Yan, Y.; Shen, Z. X.; Loh, K. P.; Tang, D. Y. *Adv. Funct. Mater.* **2009**, *19*, 3077–3083.
- (31) Sun, Z.; Hasan, T.; Torrisi, F.; Popa, D.; Privitera, G.; Wang, F.; Bonaccorso, F.; Basko, D. M.; Ferrari, A. C. *ACS Nano* **2010**, *4*, 803–810.
- (32) Winzer, T.; Knorr, A.; Mittendorff, M.; Winnerl, S.; Lien, M.-B.; Sun, D.; Norris, T. B.; Helm, M.; Malic, E. *Appl. Phys. Lett.* **2012**, *101*, 221115.
- (33) Li, H.; Zhang, Q.; Liu, C.; Xu, S.; Gao, P. *ACS Nano* **2011**, *5*, 3198–3203.
- (34) Dean, C. R.; Young, A. F.; Meric, I.; Lee, C.; Wang, L.; Sorgenfrei, S.; Watanabe, K.; Taniguchi, T.; Kim, P.; Shepard, K. L.; Hone, J. *Nat. Nanotechnol.* **2010**, *5*, 722–726.
- (35) McBryde, D.; Gow, P.; Berry, S. A.; Barnes, M. E.; Aghajani, A.; Apostolopoulos, V. *Appl. Phys. Lett.* **2014**, *104*, 201108.
- (36) Wang, Q. H.; Kalantar-Zadeh, K.; Kis, A.; Coleman, J. N.; Strano, M. S. *Nat. Nanotechnol.* **2012**, *7*, 699–712.
- (37) Koski, K. J.; Cui, Y. *ACS Nano* **2013**, *7*, 3739–3743.
- (38) Lee, S.; Lee, K.; Liu, C.-H.; Zhong, Z. *Nanoscale* **2012**, *4*, 639–644.